

# VORL-EXPLORE: A Hybrid Learning Planning Approach to Multi-Robot Exploration in Dynamic Environments

Ning Liu<sup>1</sup>, Sen Shen<sup>2</sup>, Zheng Li<sup>1</sup>, Sheng Liu<sup>3</sup>, Dongkun Han<sup>2</sup>, Shangke Lyu<sup>4\*</sup>, Thomas Braunl<sup>1</sup>

**Abstract**—Hierarchical multi-robot exploration commonly decouples frontier allocation from local navigation, which can make the system brittle in dense and dynamic environments. Because the allocator lacks direct awareness of execution difficulty, robots may cluster at bottlenecks, trigger oscillatory replanning, and generate redundant coverage. We propose VORL-EXPLORE, a hybrid learning and planning framework that addresses this limitation through execution fidelity, a shared estimate of local navigability that couples task allocation with motion execution. This fidelity signal is incorporated into a fidelity-coupled Voronoi objective with inter-robot repulsion to reduce contention before it emerges. It also drives a risk-aware adaptive arbitration mechanism between global  $A^*$  guidance and a reactive reinforcement learning policy, balancing long-range efficiency with safe interaction in confined spaces. The framework further supports online self-supervised recalibration of the fidelity model using pseudo-labels derived from recent progress and safety outcomes, enabling adaptation to non-stationary obstacles without manual risk tuning. We evaluate this capability separately in a dedicated severe-traffic ablation. Extensive experiments in randomized grids and a Gazebo factory scenario show high success rates, shorter path length, lower overlap, and robust collision avoidance. The source code will be made publicly available upon acceptance.

## I. INTRODUCTION

Large-scale multi-robot systems enable exploration and mapping in unknown environments such as warehouses and disaster response [1], [2]. In real deployments, local traversability and collision risk evolve over time due to dynamic obstacles and time-varying congestion, which makes travel time and interaction outcomes nonstationary. Routes that are feasible at one moment can become temporary bottlenecks later. Many exploration frameworks therefore adopt a hierarchical structure that separates global task allocation from local motion execution [3]. Under an ideal synchronized shared-state assumption, this design scales well because robots compute assignments and motion actions distributively.

However, the hierarchy becomes fragile when execution difficulty changes faster than the allocator can react. Fig. 1 provides a minimal static example, where robots select frontiers using distance-driven region partitioning, such as Voronoi rules induced by Breadth-First Search (BFS) distance. Distance-driven allocators work well in open space, but they can dispatch multiple robots toward adjacent frontiers that rely on the same narrow passages, which creates congestion during execution [4]. Robots may then enter

yielding oscillations and mutual blocking, repeatedly triggering local replanning [5]. In dynamic environments, this decoupling is amplified because moving obstacles and shifting traffic can invalidate previously good routes, while the upstream objective remains unchanged and keeps regenerating contested patterns. What is missing is a shared execution-fidelity signal that can be updated online and fed back to the allocator, so that target utilities reflect instantaneous navigability and interaction risk [6].

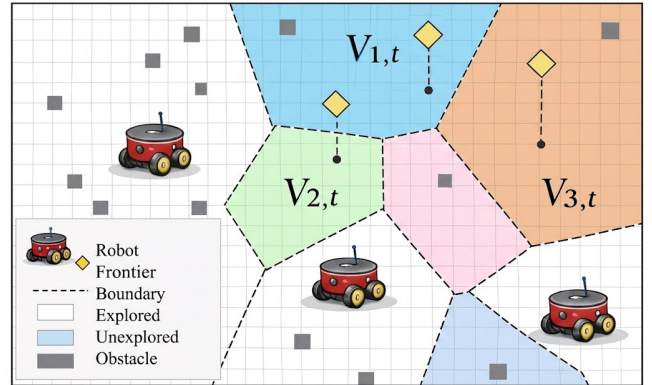


Fig. 1: Canonical Voronoi-based frontier assignment in multi-robot exploration. Three robots share an occupancy map, extract frontiers, and form a Voronoi partition  $\{V_{i,t}\}$  induced by BFS distance. Each robot selects a frontier within its region as the next exploration goal.

This hierarchy implicitly assumes that each robot can execute its assigned target reliably under local dynamics [7], [8]. As team size grows and obstacle motion increases, congestion and multi-robot interactions can slow or even stall local navigation. These execution failures do not remain local. They cascade through shared corridors, induce mutual blocking, and trigger repeated replanning [9]. Meanwhile, frontier allocators often operate without an online difficulty signal, and local controllers seldom report execution confidence upstream. This mismatch can dispatch robots to inefficient targets. It can also amplify path conflicts and redundant coverage [10].

Existing attempts to improve robustness often focus on the execution layer, using decentralized learning for collision avoidance or heuristic arbitration for short-horizon decisions [11]. Without bottom-up feedback, the allocator cannot react to local congestion, which leads to redundant travel and deadlocks in high-density settings [12].

To address these challenges, we propose VORL-EXPLORE, a hybrid learning and planning framework that

<sup>1</sup>The University of Western Australia; <sup>2</sup>The Chinese University of Hong Kong; <sup>3</sup>Karlsruhe Institute of Technology; <sup>4</sup>Nanjing University; \*Corresponding author.

couples frontier assignment with motion execution through a shared signal, execution fidelity. Each robot predicts execution fidelity from local occupancy structure and congestion cues to estimate whether reliable progress is feasible under current dynamics. This signal shapes Voronoi frontier scoring by inflating the effective cost and downweighting the utility of frontiers whose routes traverse crowded corridors, which reduces clustering at bottlenecks. It also triggers motion arbitration: robots follow global planning guidance when fidelity is high, and switch to a reactive learned policy when dense interactions make planned progress unreliable. We update the fidelity model online using self-supervised pseudo-labels derived from recent coverage gains and safety outcomes, instead of fixed hand-crafted risk rules.

The fundamental contributions are summarized as follows:

- A bidirectional closed-loop architecture is proposed to address the structural limitations of strictly top-down multi-robot exploration, unifying the task and motion layers through real-time bottom-up feedback.
- Execution fidelity is formulated as a shared, continuous representation of local navigability. This single shared signal acts as the architectural link that simultaneously modulates the macroscopic Voronoi-based task assignment and governs the microscopic motion strategy arbitration.
- A self-supervised online adaptation scheme is introduced to leverage posterior physical progress for updating the fidelity estimator in real-time. Paired with a rigorous symmetry-breaking recovery rule, this scheme ensures robust system execution without relying on manual heuristics or stationary environmental assumptions.

## II. RELATED WORK

### A. Target Assignment and Regional Partitioning

To scale frontier-based exploration [13] to large teams, decentralized assignment commonly relies on geometric partitioning, such as Voronoi cells [14], or market-based bidding [15]. Most allocators optimize map-based utility using simplified travel cost surrogates [16]. In dense teams and dynamic environments, effective execution cost can vary rapidly due to congestion, multi-robot interaction, and intermittent blockage. Several distributed exploration systems acknowledge these effects but do not explicitly provide a real-time feasibility or congestion signal to the assignment objective [17]. As a result, assignments may remain misaligned with the instantaneous navigability of the environment, which can increase redundant travel and coordination conflicts in narrow passages and crowded regions.

### B. Path Planning and Motion Execution

While classical search-based planners like A\* and D\* variants provide completeness under static assumptions [18], [19], they incur substantial replanning overhead and latency in dynamic settings with frequent obstacle motion or multi-robot interactions [20].

Learning-based reactive planners improve local efficiency by mapping observations to collision-avoidance actions, and have been widely studied for multi-robot navigation and MAPF-like settings [21]. These methods are effective for short-horizon safety and progress, but they typically operate as local policies that do not expose an explicit execution confidence estimate to the task assignment layer. In addition, policies trained offline can degrade under deployment shifts such as unseen obstacle behaviors or density regimes [22], [23]. This separation makes it difficult for the system to adjust macroscopic target priorities based on instantaneous local controllability.

### C. Connecting Assignment and Execution

Many systems preserve a cascaded hierarchy where allocation and execution are designed separately [24], which supports scalability but may lead to deadlocks or stalled coverage in narrow corridors and dense interactions [25]. Several works improve robustness within the execution layer via hybrid navigation and arbitration, for example by switching between a classical planner and a learned policy using rule-based detectors [26]. Other approaches learn coordination or communication structures for multi-robot navigation and pathfinding, often leveraging priorities from classical planners to organize local interactions [27]. However, the signals used for arbitration or coordination are rarely formulated as a shared and continuously updated variable that can directly modulate frontier assignment. Our method differs by using an online estimate of local navigability as a coupling signal that influences both frontier scoring and motion arbitration.

### D. Online Adaptation in Exploration

Online adaptation is important when obstacle motion and interaction density shift over time. Prior work studies self-supervised updates for local collision avoidance and behavior adaptation [28], as well as hierarchical navigation that combines global guidance with reactive local controllers [29], [30]. Most existing adaptation refines local execution behavior, while the coupling used by the allocator is fixed. We instead calibrate the coupling signal online using progress and safety feedback to maintain consistency under nonstationarity.

## III. PROBLEM DEFINITION

### A. Environment Model

A team of  $N$  robots explores an initially unknown grid workspace. Time is discrete with  $t \in \mathbb{N}$  and  $t = 0$  at initialization. Let  $V$  be the set of cells and  $E$  be the four-neighbor adjacency edges. Robot  $i$  is at  $x_{i,t} \in V$  and selects an action  $a_{i,t} \in \mathcal{S}_{i,t}$ , where  $\mathcal{S}_{i,t}$  contains collision-free moves that satisfy map constraints. The environment is represented by an occupancy map  $M_t : V \rightarrow \{\text{free}, \text{occ}, \text{unk}\}$ . Each robot senses within radius  $R_s$  and exchanges pose and map updates to maintain a synchronized occupancy map. This shared-map assumption is commonly adopted in frontier-based exploration systems and enables distributed decision making

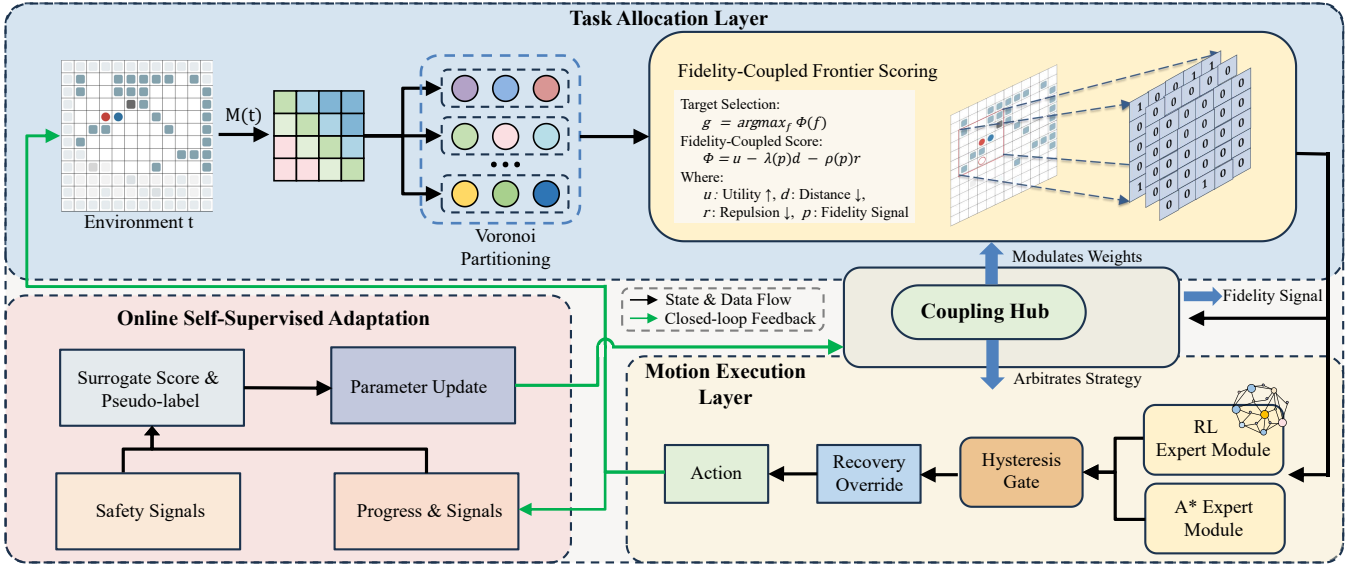


Fig. 2: Closed-loop architecture of VORL-EXPLORE. Each robot estimates execution fidelity  $p_{i,t}$  online from local cues and shared teammate states. In the task layer,  $p_{i,t}$  modulates frontier-scoring weights to reduce assignments that are likely to cause congestion. In the motion layer,  $p_{i,t}$  drives a hysteresis gate that selects between A\* guidance and a reactive RL policy. Progress and safety outcomes generate pseudo-labels to update the fidelity estimator online, closing the coupling loop.

without a centralized optimizer. We do not model delayed, lossy, or bandwidth-limited communication in this paper.

Frontiers are free cells adjacent to at least one unknown cell,  $\mathcal{F}_t = \{v \in V \mid M_t[v] = \text{free}, \exists u \in \mathcal{N}_4[v], M_t[u] = \text{unk}\}$ . Dynamic obstacles induce nonstationarity. Let  $\mathcal{O}_t \subseteq V$  denote cells occupied by dynamic obstacles at time  $t$ , moving with speed ratio  $v \in (0, 1)$  relative to robots. Robots treat  $\mathcal{O}_t$  as time-varying hard constraints within sensing range. The fused map is updated by overwriting newly observed cells and marking  $\mathcal{O}_t$  as occ.

### B. Objective

Let  $t^*$  be the first time when no frontiers remain,  $t^* = \inf\{t \in \mathbb{N} \mid \mathcal{F}_t = \emptyset\}$ . Define the team-level coverage multiplicity  $\kappa[v] = |\{i \mid \exists t < t^*, x_{i,t} = v\}|$ . Redundant overlap is the fraction of visited cells covered by at least two robots,

$$\Omega = \frac{|\{v \in V \mid \kappa[v] \geq 2\}|}{|\{v \in V \mid \kappa[v] \geq 1\}|}. \quad (1)$$

We minimize a weighted sum of completion time and redundancy,

$$J = \alpha t^* + \lambda_\Omega \Omega, \quad \alpha \gg \lambda_\Omega \geq 0, \quad (2)$$

by designing decentralized policies  $\{\pi_i\}_{i=1}^N$  that use the shared global map to compute target selection and motion decisions independently.

## IV. METHODOLOGY

This work presents a closed-loop multi-robot exploration framework that couples frontier assignment and motion execution through a shared execution fidelity signal  $p_{i,t}$ . Execution fidelity is a lightweight planner-selection score that reflects whether robot  $i$  is likely to make progress with

globally guided navigation under the current local interactions. The same signal modulates the frontier scoring rule in the task layer and drives strategy arbitration in the execution layer. During training rollouts, progress and safety outcomes provide self-supervision to update the fidelity estimator, forming a bidirectional feedback loop between allocation and control. Fig. 2 provides an overview of the architecture and highlights the two coupling links between the task layer and the motion layer. Let  $g_{i,t} \in \mathcal{F}_t \cup \{\emptyset\}$  denote the assigned frontier target for robot  $i$  at decision step  $t$ , and let  $p_{i,t} \in [0, 1]$  denote the execution-fidelity score used for planner selection. Two step intervals,  $\Delta_{as}$  and  $\Delta_{up}$ , are used for task reassignment and online parameter updates, respectively. Task reassignment is executed every  $\Delta_{as}$  decision steps and is additionally triggered immediately when robot  $i$  reaches its current goal, i.e.,  $x_{i,t} = g_{i,t-1}$ , or when no valid goal is available ( $g_{i,t-1} = \emptyset$ ). During execution, the reactive policy uses local observations  $o_{i,t}$  within a sensing radius  $R_s$  (in grid cells), while inter-robot repulsion considers teammates within an interaction radius  $R_u$  defined in grid distance. A fixed window length  $W$  maintains the history buffer  $\mathcal{H}_{i,t}$  for online adaptation.

### A. Closed-loop architecture

Each robot exchanges map updates with teammates to maintain an approximately consistent shared occupancy map. At each time step, a global frontier candidate set  $\mathcal{F}_t$  is extracted. Subsequently, a Voronoi partition induced by the robots' current poses filters this set into a robot-specific subset  $\mathcal{F}_{i,t} \subseteq \mathcal{F}_t$ . The target  $g_{i,t}$  is then assigned by maximizing a fidelity-coupled objective  $\Phi_{i,t}[f]$  over  $f \in \mathcal{F}_{i,t}$ . To evaluate this objective, the shortest-path distance  $d_{i,t}[f]$  for each candidate is computed via Breadth-First Search (BFS)

on the free-space grid. Concurrently, the robot estimates an execution fidelity score  $p_{i,t}$  derived from lightweight local features, including occupancy, congestion, and recent progress. This target assignment is refreshed periodically or triggered asynchronously by significant map updates and recovery activations. Notably, inter-robot repulsion is exclusively evaluated during these reassignment rounds to formulate  $\Phi_{i,t}[f]$ , rather than during per-step motion execution. The assigned target is then pursued via a fidelity-gated arbitration strategy. The resulting progress and safety outcomes provide continuous self-supervision to update the fidelity estimator online. Algorithm 1 summarizes this closed-loop procedure, with detailed formulations provided in subsequent sections.

---

**Algorithm 1:** Fidelity-Gated Coupled Exploration

---

**Input:**  $x_{i,t}, M_t, o_{i,t}, g_{i,t-1}, \mathcal{H}_{i,t}$ ; shared  $\{x_{j,t}, g_{j,t-1}\}$ ;  
 $R_s, R_u, \Delta_{as}, \Delta_{up}$   
**Output:**  $g_{i,t}$  and  $a_{i,t}$

- 1 Update shared state with  $(x_{i,t}, g_{i,t-1})$
- 2  $z_{i,t} \leftarrow \phi(M_t, x_{i,t}, o_{i,t}, \{x_{j,t}\}, \{g_{j,t-1}\}, \mathcal{H}_{i,t})$
- 3  $p_{i,t} \leftarrow \sigma(w_i^\top z_{i,t} + b_i)$
- 4 Update  $(c_{i,t}^H, c_{i,t}^L, s_{i,t})$
- 5 **if**  $t \bmod \Delta_{as} = 0$  **or**  $g_{i,t-1} = \emptyset$  **or**  $x_{i,t} = g_{i,t-1}$  **then**
- 6      $\mathcal{F}_t \leftarrow \text{FRONTIERS}(M_t)$ ;
- 7      $g_{i,t} \leftarrow \arg \max_{f \in \mathcal{F}_t} \Phi_{i,t}[f]$ ;
- 8 **else**
- 9      $g_{i,t} \leftarrow g_{i,t-1}$
- 10  $(a_{i,t}^A, ok) \leftarrow \text{PLANAR}^*(M_t, x_{i,t}, g_{i,t})$
- 11 **if**  $\neg ok$  **then**
- 12      $a_{i,t}^A \leftarrow \text{safe no-op}$
- 13      $s_{i,t} \leftarrow 0$
- 14  $a_{i,t}^E \leftarrow \text{RL}(o_{i,t})$
- 15 **if**  $s_{i,t} = 1$  **then**
- 16      $\tilde{a}_{i,t} \leftarrow a_{i,t}^A$
- 17 **else**
- 18      $\tilde{a}_{i,t} \leftarrow a_{i,t}^E$
- 19  $a_{i,t} \leftarrow \text{RECOVERYOVERRIDE}(\tilde{a}_{i,t}, \mathcal{H}_{i,t})$
- 20 **if**  $t \bmod \Delta_{up} = 0$  **then**
- 21     Compute  $(Q_{i,t}, \tilde{y}_{i,t})$
- 22     Update  $(w_i, b_i)$

---

### B. Coupled frontier assignment

The task layer selects a frontier target from  $\mathcal{F}_t$  while accounting for execution reliability. Each frontier  $f$  is associated with an exploration utility  $u_t[f]$  that reflects expected information gain.  $u_t[f]$  is defined as the number of unknown cells within a sensing-radius neighborhood around  $f$ ,

$$u_t[f] = |\{v \in \mathcal{B}(f, R_s) \mid M_t[v] = \text{unk}\}|, \quad (3)$$

where  $\mathcal{B}(f, R_s)$  denotes grid cells within radius  $R_s$  of  $f$ .

The assignment also accounts for travel cost and interaction risk. We introduce a repulsion penalty  $r_{i,t}[f]$  to discourage assigning multiple robots to nearby frontiers that may trigger local crowding and corridor conflicts. Execution fidelity  $p_{i,t}$  continuously modulates the balance among utility, distance, and repulsion. When  $p_{i,t}$  is high,  $\lambda(\cdot)$  and  $\rho(\cdot)$  remain small and the utility term dominates the trade

off. When  $p_{i,t}$  is low, the distance and repulsion penalties increase, which biases the assignment toward nearby and low conflict frontiers under congestion and dynamic obstacles. The coupled score is

$$\Phi_{i,t}[f] = u_t[f] - \lambda(p_{i,t}) d_{i,t}[f] - \rho(p_{i,t}) r_{i,t}[f]. \quad (4)$$

Within each reassignment round, we apply min-max normalization to  $u_t[f]$ ,  $d_{i,t}[f]$ , and  $r_{i,t}[f]$  over the current frontier set before computing  $\Phi_{i,t}[f]$ .

To reduce corridor conflicts, the repulsion penalty of assigning robot  $i$  to frontier  $f$  is defined as

$$r_{i,t}[f] = \frac{1}{N-1} \sum_{j \neq i} \mathbf{1}\{d_t(f, x_{j,t}) \leq R_u\} \exp\left(-\frac{d_t(f, x_{j,t})}{\sigma_x}\right) + \frac{\beta}{N-1} \sum_{j \neq i} \mathbf{1}\{d_t(f, g_{j,t-1}) \leq R_u\} \exp\left(-\frac{d_t(f, g_{j,t-1})}{\sigma_g}\right), \quad (5)$$

where  $d_t(\cdot, \cdot)$  denotes the same BFS shortest-path distance used to compute  $d_{i,t}[f]$  on the current free-space grid induced by  $M_t$ . For the target-based term, the indicator is treated as false when  $g_{j,t-1} = \emptyset$ , so that contribution is zero.  $\sigma_x$  and  $\sigma_g$  control the interaction range and  $\beta$  balances pose-based and target-based repulsion.

The weights increase as fidelity decreases and a simple linear form is used

$$\lambda(p_{i,t}) = \lambda_0 + \lambda_1(1 - p_{i,t}), \quad \rho(p_{i,t}) = \rho_0 + \rho_1(1 - p_{i,t}). \quad (6)$$

The robot selects the frontier with maximal  $\Phi_{i,t}[f]$  and re-evaluates upon periodic refresh or event triggers. This design removes the fragile assumption of reliable execution and injects local feasibility into allocation through a shared continuous signal.

### C. Motion arbitration with a learnable switch

The execution layer produces two complementary actions. A planner generates a globally guided action  $a_{i,t}^A$  toward the assigned target using the shared map, while a reactive policy outputs  $a_{i,t}^E$  directly from local observations. A lightweight learnable gate outputs an execution-fidelity score  $p_{i,t}$ , indicating whether globally guided execution is expected to remain reliable under the current local dynamics. The gate is implemented as logistic regression to support decentralized online adaptation,

$$p_{i,t} = \sigma\left(w_i^\top z_{i,t} + b_i\right), \quad z_{i,t} \in \mathbb{R}^8, \quad (7)$$

where  $\sigma(\cdot)$  denotes the sigmoid function. The feature vector is produced by a deterministic extractor

$$z_{i,t} = \phi\left(M_t, x_{i,t}, o_{i,t}, \{x_{j,t}\}_{j \neq i}, \{g_{j,t-1}\}_{j \neq i}, \mathcal{H}_{i,t}\right) \in \mathbb{R}^8, \quad (8)$$

where  $\phi(\cdot)$  returns a compact set of interpretable statistics computed from the occupancy and unknown grids, the feasibility filter, shared teammate states, and a short history buffer  $\mathcal{H}_{i,t}$  over the most recent  $W$  steps. Concretely,  $z_{i,t}$  consists of exactly eight lightweight statistics: local crowding measured by the count of nearby teammates within radius  $R_u$  in the

shared state, a short-horizon stuck flag, normalized distance to the assigned frontier, feasible-action ratio, unknown-area ratios around the robot and around the goal, local block-age density from four-neighbor free cells, and a planner-feasibility flag indicating whether the  $A^*$  branch returns a valid action.

A binary switch state  $s_{i,t} \in \{0, 1\}$  is used, where  $s_{i,t} = 1$  selects the planner branch and  $s_{i,t} = 0$  selects the reactive policy. To reduce oscillatory switching, the hysteresis mechanism uses two thresholds,  $\tau_H$  and  $\tau_L$ , with  $\tau_H > \tau_L$ , together with a dwell length  $K$ . Two counters accumulate consecutive threshold satisfaction,

$$c_{i,t}^H = \mathbb{I}\{p_{i,t} \geq \tau_H\} (c_{i,t-1}^H + 1), \quad c_{i,t}^L = \mathbb{I}\{p_{i,t} \leq \tau_L\} (c_{i,t-1}^L + 1), \quad (9)$$

and the switch updates only after  $K$  consistent steps,

$$s_{i,t} = \begin{cases} 1, & s_{i,t-1} = 0 \wedge c_{i,t}^H \geq K, \\ 0, & s_{i,t-1} = 1 \wedge c_{i,t}^L \geq K, \\ s_{i,t-1}, & \text{otherwise.} \end{cases} \quad (10)$$

This yields a preliminary action

$$\tilde{a}_{i,t} = \begin{cases} a_{i,t}^A, & s_{i,t} = 1, \\ a_{i,t}^E, & s_{i,t} = 0. \end{cases} \quad (11)$$

Finally, a recovery override enforces safety and breaks stagnation. It triggers on planning infeasibility, stalled progress over  $W$  steps, or frequent switch oscillation, executes a short symmetry-breaking maneuver, and then resumes normal gated execution.

#### D. Online self-supervised adaptation

The gate is updated online without manual labels so that the switch remains calibrated in unseen environments. After execution, a surrogate quality score  $Q_{i,t}$  is computed over a short sliding window of length  $W$ :

$$Q_{i,t} = \omega_{\text{cov}} \Delta \text{cov}_{i,t} + \omega_{\text{dist}} \Delta \text{dist}_{i,t} - \omega_{\text{risk}} \text{risk}_{i,t} - \omega_{\text{stall}} \text{stall}_{i,t}. \quad (12)$$

where  $\omega_* > 0$  are fixed weights. To match the planning layer,  $\Delta \text{dist}_{i,t}$  uses the BFS shortest-path distance on the current occupancy grid, so necessary obstacle detours are not penalized.  $\Delta \text{cov}_{i,t}$  counts newly observed cells,  $\text{risk}_{i,t}$  aggregates collisions and constraint violations, and  $\text{stall}_{i,t}$  penalizes lack of progress.

A pseudo label is generated from the score using the indicator function  $\mathbb{I}\{\cdot\}$ :

$$\tilde{y}_{i,t} = \mathbb{I}\{Q_{i,t} \geq 0\}. \quad (13)$$

The local gate is trained with regularized binary cross entropy loss, where  $\lambda_{\text{reg}}$  controls the L2 regularization:

$$\mathcal{L}_{i,t} = -\tilde{y}_{i,t} \log p_{i,t} - (1 - \tilde{y}_{i,t}) \log \{1 - p_{i,t}\} + \frac{\lambda_{\text{reg}}}{2} \|w_i\|_2^2. \quad (14)$$

Updates are applied only when the score magnitude exceeds a clear margin  $m > 0$  to reduce noise driven drift. A single

online step with learning rate  $\eta$  is:

$$w_i \leftarrow w_i - \eta \mathbb{I}\{|Q_{i,t}| \geq m\} \left( \{p_{i,t} - \tilde{y}_{i,t}\} z_{i,t} + \lambda_{\text{reg}} w_i \right), \quad (15)$$

$$b_i \leftarrow b_i - \eta \mathbb{I}\{|Q_{i,t}| \geq m\} \{p_{i,t} - \tilde{y}_{i,t}\}. \quad (16)$$

This mechanism enables the learnable switch to track changing local dynamics and maintain coherent allocation and execution behavior.

## V. EXPERIMENTS

### A. Experimental Setup and Baselines

1) *Training and Environment*: We implement the reactive RL execution policy  $\pi^E$  using the EPOM design [31] and train it with PPO using a learning rate of  $1 \times 10^{-4}$  and discount factor  $\gamma = 0.99$ . All policy parameters are trained from scratch on procedurally generated  $64 \times 64$  grids with  $N = 64$  robots and a horizon of 512 steps. Static obstacles are sampled independently per cell with occupancy probability  $p_{\text{occ}} \sim \mathcal{U}[0.15, 0.45]$  to induce large-scale coordination under varying obstacle densities. We set the sensing radius and interaction radius to  $R_s = 3$  and  $R_u = 3$  cells. Dynamic obstacles move at a fixed speed ratio  $v = 0.5$  relative to the robot speed in all experiments.

The logistic gate is warm-started using self-supervised rollouts collected in the same procedural environments and under the same robot density. In all main comparison experiments, we freeze the gate parameters at test time and use a fixed checkpoint to ensure fair comparison and reproducibility. Test-time gate updates are disabled unless otherwise stated, and are evaluated only in the dedicated severe-traffic ablation of Table II.

Evaluation uses held-out  $40 \times 40$  and  $80 \times 80$  grids with 30% static obstacle density. To examine scalability and congestion effects, we vary both the number of dynamic obstacles and the team size across scenarios. The episode horizon scales with map size to control for size-dependent effects. All hyperparameters remain fixed during testing.

2) *Evaluation Protocol and Baselines*: Evaluation uses all methods under a decoupled two-stage exploration pipeline with a unified protocol. All methods share the same discrete action space, feasibility filter  $\mathcal{S}_{i,t}$ , horizon  $T_{\text{max}}$ , and reassignment schedule. At the protocol level, we assume ideal shared-state communication to maintain a synchronized occupancy map for frontier extraction and goal assignment. In executor-level evaluation, all learning-based executors, including VORL-EXPLORE, act only on local observations and do not access the global map or any teammate states.

We separate the baselines into allocator-level and executor-level groups because most execution methods operate through a frontier-goal interface. In the allocator-level comparison, only the module that selects  $g_{i,t} \in \mathcal{F}_t$  is replaced, while the execution module remains fixed to that of VORL-EXPLORE. We compare greedy frontier assignment [32], Hungarian matching [33], and auction-based allocation [15].

In the executor-level comparison, the allocator and the reassignment schedule are fixed. At each reassignment step, all methods receive the same frontier goal  $g_{i,t}$ , and only the

TABLE I: Experimental results on  $40 \times 40$  and  $80 \times 80$  grids over 100 runs. Values are reported as mean  $\pm$  standard deviation. SR: success rate ( $\uparrow$ ), EL: Exploration length ( $\downarrow$ ), and Overlap: redundant overlap ratio ( $\downarrow$ ). Best values are **bolded**.

Method	8 Dynamic obstacles			16 Dynamic obstacles			32 Dynamic obstacles			64 Dynamic obstacles		
	SR $\uparrow$	EL $\downarrow$	Overlap $\downarrow$	SR $\uparrow$	EL $\downarrow$	Overlap $\downarrow$	SR $\uparrow$	EL $\downarrow$	Overlap $\downarrow$	SR $\uparrow$	EL $\downarrow$	Overlap $\downarrow$
• $40 \times 40$ world, 4 Agents, 30% static obstacle density												
DHC	0.90 $\pm$ 0.08	169.22 $\pm$ 11.3	0.23 $\pm$ 0.03	0.88 $\pm$ 0.09	171.78 $\pm$ 12.1	0.23 $\pm$ 0.03	0.87 $\pm$ 0.10	179.64 $\pm$ 14.5	0.23 $\pm$ 0.03	0.88 $\pm$ 0.09	191.45 $\pm$ 15.2	0.24 $\pm$ 0.04
PICO	0.71 $\pm$ 0.12	212.80 $\pm$ 18.4	0.32 $\pm$ 0.05	0.62 $\pm$ 0.15	213.60 $\pm$ 19.1	0.32 $\pm$ 0.05	0.56 $\pm$ 0.14	221.40 $\pm$ 20.3	0.33 $\pm$ 0.06	0.51 $\pm$ 0.16	231.42 $\pm$ 21.5	0.33 $\pm$ 0.06
MATS-LP	0.85 $\pm$ 0.09	198.75 $\pm$ 14.2	0.26 $\pm$ 0.04	0.82 $\pm$ 0.10	203.12 $\pm$ 15.4	0.26 $\pm$ 0.04	0.85 $\pm$ 0.11	205.33 $\pm$ 16.1	0.27 $\pm$ 0.05	0.87 $\pm$ 0.10	207.84 $\pm$ 17.5	0.25 $\pm$ 0.04
ICBS	0.78 $\pm$ 0.11	182.20 $\pm$ 13.1	0.27 $\pm$ 0.04	0.68 $\pm$ 0.14	194.40 $\pm$ 16.5	0.29 $\pm$ 0.05	0.48 $\pm$ 0.16	218.30 $\pm$ 22.4	0.35 $\pm$ 0.07	0.22 $\pm$ 0.18	235.60 $\pm$ 30.2	0.41 $\pm$ 0.09
VORL-A*	0.91 $\pm$ 0.07	170.50 $\pm$ 10.2	0.24 $\pm$ 0.03	0.84 $\pm$ 0.09	182.30 $\pm$ 14.4	0.26 $\pm$ 0.04	0.68 $\pm$ 0.13	204.40 $\pm$ 21.5	0.31 $\pm$ 0.06	0.44 $\pm$ 0.15	225.60 $\pm$ 28.1	0.36 $\pm$ 0.08
VORL-RL	0.81 $\pm$ 0.10	185.20 $\pm$ 15.5	0.27 $\pm$ 0.05	0.83 $\pm$ 0.09	182.60 $\pm$ 14.2	0.26 $\pm$ 0.04	0.87 $\pm$ 0.08	178.10 $\pm$ 12.5	0.24 $\pm$ 0.04	0.89 $\pm$ 0.08	184.50 $\pm$ 13.1	0.23 $\pm$ 0.04
VORL-EXPLORE	<b>0.94<math>\pm</math>0.06</b>	<b>165.35<math>\pm</math>9.8</b>	<b>0.21<math>\pm</math>0.02</b>	<b>0.92<math>\pm</math>0.07</b>	<b>168.42<math>\pm</math>10.3</b>	<b>0.22<math>\pm</math>0.02</b>	<b>0.94<math>\pm</math>0.06</b>	<b>174.01<math>\pm</math>10.8</b>	<b>0.21<math>\pm</math>0.02</b>	<b>0.95<math>\pm</math>0.05</b>	<b>182.39<math>\pm</math>11.9</b>	<b>0.21<math>\pm</math>0.02</b>
• $80 \times 80$ world, 16 Agents, 30% static obstacle density												
DHC	0.99 $\pm$ 0.01	186.94 $\pm$ 15.5	0.32 $\pm$ 0.04	0.96 $\pm$ 0.03	188.37 $\pm$ 16.1	0.32 $\pm$ 0.04	0.91 $\pm$ 0.05	188.41 $\pm$ 16.2	0.33 $\pm$ 0.05	0.87 $\pm$ 0.07	193.02 $\pm$ 17.5	0.34 $\pm$ 0.05
PICO	0.52 $\pm$ 0.14	287.24 $\pm$ 25.4	0.47 $\pm$ 0.07	0.51 $\pm$ 0.15	292.42 $\pm$ 26.8	0.48 $\pm$ 0.08	0.49 $\pm$ 0.14	293.39 $\pm$ 27.1	0.48 $\pm$ 0.07	0.42 $\pm$ 0.16	303.52 $\pm$ 30.2	0.49 $\pm$ 0.09
MATS-LP	0.93 $\pm$ 0.06	219.34 $\pm$ 18.5	0.36 $\pm$ 0.05	0.91 $\pm$ 0.07	222.88 $\pm$ 19.3	0.37 $\pm$ 0.06	0.86 $\pm$ 0.08	227.27 $\pm$ 20.8	0.36 $\pm$ 0.05	0.88 $\pm$ 0.08	234.15 $\pm$ 21.4	0.36 $\pm$ 0.05
ICBS	0.85 $\pm$ 0.09	205.50 $\pm$ 17.3	0.36 $\pm$ 0.05	0.69 $\pm$ 0.12	222.40 $\pm$ 21.7	0.41 $\pm$ 0.07	0.52 $\pm$ 0.14	248.30 $\pm$ 28.1	0.45 $\pm$ 0.08	0.31 $\pm$ 0.16	278.60 $\pm$ 34.5	0.51 $\pm$ 0.10
VORL-A*	0.96 $\pm$ 0.04	188.50 $\pm$ 14.8	0.33 $\pm$ 0.04	0.88 $\pm$ 0.07	202.20 $\pm$ 18.1	0.35 $\pm$ 0.05	0.72 $\pm$ 0.11	228.40 $\pm$ 24.5	0.40 $\pm$ 0.07	0.55 $\pm$ 0.13	252.80 $\pm$ 29.2	0.44 $\pm$ 0.08
VORL-RL	0.86 $\pm$ 0.09	203.20 $\pm$ 18.4	0.35 $\pm$ 0.05	0.88 $\pm$ 0.08	196.40 $\pm$ 16.8	0.34 $\pm$ 0.04	0.90 $\pm$ 0.07	190.60 $\pm$ 15.5	0.33 $\pm$ 0.04	0.92 $\pm$ 0.06	193.20 $\pm$ 16.2	0.32 $\pm$ 0.04
VORL-EXPLORE	<b>0.99<math>\pm</math>0.01</b>	<b>181.32<math>\pm</math>12.6</b>	<b>0.30<math>\pm</math>0.03</b>	<b>0.98<math>\pm</math>0.01</b>	<b>182.71<math>\pm</math>13.1</b>	<b>0.31<math>\pm</math>0.03</b>	<b>0.96<math>\pm</math>0.02</b>	<b>184.47<math>\pm</math>14.2</b>	<b>0.31<math>\pm</math>0.03</b>	<b>0.96<math>\pm</math>0.02</b>	<b>188.40<math>\pm</math>14.6</b>	<b>0.31<math>\pm</math>0.03</b>

local execution module that maps  $(o_{i,t}, g_{i,t})$  to an action is replaced. To enforce a unified interface, actions are filtered by the same feasibility set  $\mathcal{S}_{i,t}$ , and executors do not access the global map or teammate states. We benchmark MATS-LP [34], DHC [22], PICO [27], and ICBS [35] using their published hyperparameters, adapting only environment-specific interface parameters such as grid size and resolution, the discrete action set, collision-checking rules, and the episode horizon. Finally, we include two ablated variants, VORL-A\* and VORL-RL, to isolate the contribution of the gating mechanism.

## B. Results

1) *Target Allocation and Scalability*: We evaluate scalability by varying the team size on an  $80 \times 80$  grid with 16 dynamic obstacles and 30% static obstacle density. Fig. 3 reports success rate and exploration length over successful runs. Auction, Hungarian, and frontier based allocators improve as the number of robots increases at first, then show diminishing returns. These methods score targets largely by static travel distance, so they do not account for congestion and moving obstacles during execution in narrow passages. As the team grows, multiple robots are dispatched toward adjacent frontiers, which increases mutual blocking and redundant travel. The frontier based baseline achieves the lowest success rates and shows little reduction in exploration length. Auction is the strongest decoupled baseline but still plateaus at an exploration length of 42.2 at maximum team size. In contrast, VORL-EXPLORE exhibits rapid and continuous convergence in exploration efficiency. Its EL drops dramatically to 25.4, and its corresponding SR curve achieves a robust 100% significantly earlier than all tested baselines. By integrating global target assignment with local reinforcement-learning execution, the system dynamically anticipates local congestion. Rather than assigning multiple robots to adjacent frontiers in congested areas, VORL-EXPLORE modulates target selection using execution fidelity, which promotes better spatial dispersion and more consistent marginal gains as team size increases.

2) *Motion Execution Performance*: Table I compares motion execution on  $40 \times 40$  and  $80 \times 80$  grids under increasing

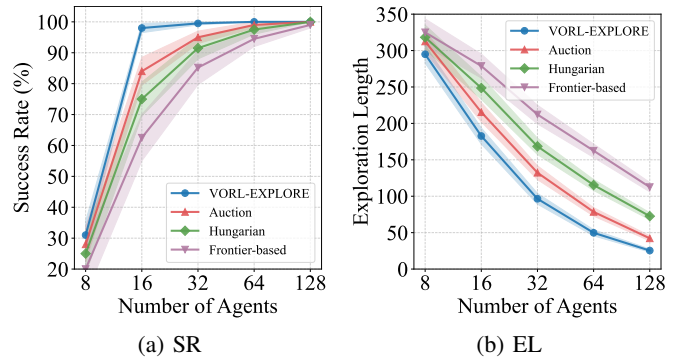


Fig. 3: Allocator-level comparison with target allocation baselines on an  $80 \times 80$  grid with 16 dynamic obstacles and 30% static obstacle density. All methods share the same VORL-EXPLORE execution layer. Curves show the mean over 100 runs and shaded regions indicate 95% confidence intervals.

numbers of dynamic obstacles. The table reports values as mean  $\pm$  standard deviation. On  $40 \times 40$  with 64 dynamic obstacles, VORL-EXPLORE achieves SR 0.95 with Overlap 0.21, while PICO drops to SR 0.51 with Overlap 0.33. On  $80 \times 80$ , the gap widens under dense traffic. VORL-EXPLORE maintains SR 0.96 at 64 dynamic obstacles, whereas ICBS declines from SR 0.85 at 8 obstacles to SR 0.31 at 64 obstacles, and Overlap increases from 0.36 to 0.51. PICO also remains low at SR 0.42 at 64 obstacles, which is consistent with deadlocks in crowded corridors. In contrast, VORL-EXPLORE sustains success rates above 90% with low redundant revisits across traffic levels, which indicates robust execution when congestion increases and baseline methods degrade.

Table I also includes two single executor variants to contextualize the hybrid switch. VORL-A\* is effective in light traffic but its SR decreases with congestion, reaching 0.55 on the  $80 \times 80$  maps with 64 dynamic obstacles. VORL-RL remains robust at high density and reaches SR 0.92 under the same setting, but it incurs longer exploration in sparse layouts. On  $80 \times 80$  with 8 dynamic obstacles, VORL-RL yields EL 203.20, while VORL-EXPLORE reduces this to EL 181.32. By selecting between planning guidance and re-

active avoidance using execution fidelity, VORL-EXPLORE achieves strong performance across both sparse and highly congested regimes. These trends indicate robust execution as traffic increases, without introducing additional online computation beyond the per-step gate evaluation.

### C. Ablation Study

Table I already reports two single-executor variants, VORL-A\* and VORL-RL, which enforce planning-only or policy-only execution and therefore isolate the effect of gate-based arbitration. Here we focus on the remaining design factors. We progressively enable the two coupling links, CA and CP, in Fig. 4, and we evaluate warm-start initialization and online adaptation of the execution fidelity estimator in Table II under heavy traffic.

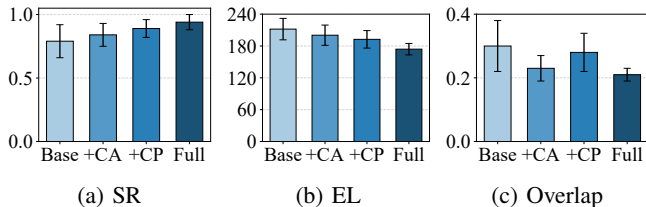


Fig. 4: Progressive ablation of the coupled architecture. Base disables both coupling links and uses decoupled target assignment and motion execution. CA enables fidelity-coupled assignment by using execution fidelity to reweight frontier scoring, while keeping the execution module unchanged. CP enables fidelity-gated switching in the execution layer, while keeping the assignment objective unchanged. Full enables both CA and CP. Bars show the mean and error bars indicate  $\pm$ STD over 100 runs with 4 agents on a  $40 \times 40$  grid, 30% static obstacle density, and 32 dynamic obstacles.

1) *Impact of the Coupled Architecture:* We compare four variants, *Base*, Coupled Planning (CP), Coupled Assignment (CA), and *Full*. *Base* decouples assignment and execution, so the allocator relies on simplified travel costs while the executor must resolve congestion and moving obstacles. *CA* couples assignment with execution fidelity, which downweights frontiers that are likely to induce detours and interference. *CP* enables gate driven switching between planning and the reactive policy, which reduces local deadlocks when crowding patterns change. *Full* enables both links. Fig. 4 shows that each link improves success and reduces both exploration length and overlap, and *Full* provides the most stable behavior across runs.

2) *Effectiveness of Online Adaptation:* We evaluate the gate initialization and online-update strategies in a severe traffic regime on a  $40 \times 40$  grid with 128 dynamic obstacles. Frequent encounters rapidly change local navigability, making a fixed predictor prone to miscalibration and repeated no-progress behavior. Table II reports mean  $\pm$  STD over 100 runs. Without pre-training or online updates, the cold static gate attains SR 0.36, triggers recovery 82.4 times per episode, and selects the planner for 91.5% of steps, indicating over-reliance on planning under congestion. Warm initialization alone improves robustness, raising SR to 0.51

and reducing recovery to 42.7, but the gate remains fixed and still over-selects planning at 74.2%. Enabling online updates yields a substantially larger gain. Even without pre-training, the cold adaptive variant increases SR to 0.65 while reducing recovery to 12.3 and planner selection to 37.8%, showing that test-time updates effectively recalibrate the gate to the current traffic conditions. Combining warm initialization with online updates further improves SR to 0.69 and achieves the lowest recovery 6.8 with planner selection 34.5%. Overall, pre-training provides a better starting point, whereas online adaptation is the dominant factor that maintains calibration under non-stationary interactions, reducing both excessive planning and recovery usage.

TABLE II: Ablation of gate initialization (Pre-train) and test-time gate updates (Online) under severe traffic. Values are mean  $\pm$  STD over 100 runs on a  $40 \times 40$  grid with 30% static obstacles and 128 dynamic obstacles.

Variant	Setup		Metrics			
	Pre-train	Online	SR $\uparrow$	EL $\downarrow$	Recov. $\downarrow$	$\pi_{\text{plan}}$ (%)
VORL <sub>Static</sub> (Cold)	×	×	0.36 $\pm$ 0.11	248.2 $\pm$ 29.5	82.4 $\pm$ 15.2	91.5
VORL <sub>Static</sub> (Warm)	✓	×	0.51 $\pm$ 0.13	224.5 $\pm$ 22.1	42.7 $\pm$ 9.6	74.2
VORL <sub>Adapt</sub> (Cold)	×	✓	0.65 $\pm$ 0.07	208.7 $\pm$ 17.5	12.3 $\pm$ 4.2	37.8
<b>VORL-EXPLORE</b>	✓	✓	<b>0.69<math>\pm</math>0.05</b>	<b>204.3<math>\pm</math>14.2</b>	<b>6.8<math>\pm</math>2.1</b>	<b>34.5</b>

### D. Experimental Validation

To examine the behavior of our approach beyond grid-world benchmarks, we conduct a proof-of-concept study in the Gazebo simulator using four Pioneer3 robots in a cluttered factory-like environment. The scene contains static obstacles and two pedestrians moving at constant velocities, which introduces persistent local nonstationarity. Under the same synchronized shared-state assumption used throughout this paper, and without any additional fine-tuning beyond the initial grid-based training, VORL-EXPLORE enables the team to expand the explored region continuously. As illustrated by the representative snapshots in Fig. 5, the robots maintain collision-free motion and avoid prolonged deadlocks while adapting their trajectories in response to moving pedestrians.

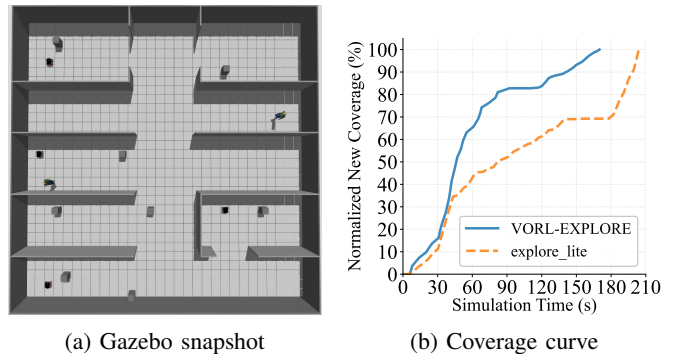


Fig. 5: Gazebo validation with four Pioneer3 robots in a dynamic factory environment. The normalized new coverage curve shows faster exploration than ROS `explore_lite`.

Exploration efficiency is further quantified by reporting

the normalized new coverage over time. Results are compared against the standard ROS explore\_lite baseline under the same dynamic conditions. The curves in Fig. 5 show that VORL-EXPLORE achieves earlier gains in normalized new coverage and sustains a higher coverage rate over the episode, which is consistent with improved exploration efficiency in this scenario. These qualitative behaviors and coverage trends suggest that the coupled architecture remains effective in a dynamic simulated setting under synchronized shared-state communication.

## VI. CONCLUSION

This paper proposes VORL-EXPLORE, a decentralized hybrid learning-and-planning framework for multi-robot exploration in dynamic environments. The core contribution is execution fidelity, a shared online estimate of local navigability that couples frontier assignment with motion execution. Fidelity modulates frontier scoring with inter-robot repulsion and drives a hysteresis switch between  $A^*$  guidance and a reactive RL policy, enabling efficient motion in open space and robust progress under dense traffic. Under the synchronized shared-state assumption adopted in this paper, benchmarks and a Gazebo factory study show higher success and lower redundancy, while ablations confirm increasing benefits with higher density and larger teams.

## REFERENCES

- [1] C. Zhu, M. Dastani, and S. Wang, "A survey of multi-agent deep reinforcement learning with communication," *Autonomous Agents and Multi-Agent Systems*, vol. 38, no. 1, p. 4, 2024.
- [2] N. Liu, S. Shen, X. Kong, H. Zhang, and T. Bräunl, "Cooperative hybrid multi-agent pathfinding based on shared exploration maps," *Journal of Intelligent & Robotic Systems*, vol. 111, p. 97, 2025.
- [3] B. Zhou, Y. Zhang, X. Chen, and S. Shen, "Fuel: Fast uav exploration using incremental frontier structure and hierarchical planning," *IEEE Robotics and Automation Letters*, vol. 6, no. 2, pp. 779–786, 2021.
- [4] A. Pierson, W. Schwarting, S. Karaman, and D. Rus, "Weighted buffered voronoi cells for distributed semi-cooperative behavior," in *IEEE International Conference on Robotics and Automation*, 2020, pp. 5611–5617.
- [5] J. Tordesillas and J. P. How, "MADER: Trajectory planner in multi-agent and dynamic environments," *IEEE Transactions on Robotics*, vol. 38, no. 1, pp. 463–476, 2022.
- [6] J. Liang, Y. Cao, Y. Ma, H. Zhao, and G. Sartoretti, "Hdplanner: Advancing autonomous deployments in unknown environments through hierarchical decision networks," *IEEE Robotics and Automation Letters*, 2024.
- [7] G. Niu, Q. Yang, Y. Gao, and M.-O. Pun, "Vision-based autonomous landing for unmanned aerial and ground vehicles cooperative systems," *IEEE Robotics and Automation Letters*, vol. 7, no. 3, pp. 6234–6241, 2021.
- [8] Y. Huang, X. Lin, and B. Englot, "Multi-robot autonomous exploration and mapping under localization uncertainty with expectation-maximization," in *IEEE International Conference on Robotics and Automation*. IEEE, 2024, pp. 7236–7242.
- [9] Y. Cai, X. He, H. Guo, W.-Y. Yau, and C. Lv, "Transformer-based multi-agent reinforcement learning for generalization of heterogeneous multi-robot cooperation," in *IEEE/RSJ International Conference on Intelligent Robots and Systems*. IEEE, 2024, pp. 13 695–13 702.
- [10] P.-Y. Lajoie, B. Ramtoula, Y. Chang, L. Carlone, and G. Beltrame, "Door-slam: Distributed, online, and outlier resilient slam for robotic teams," *IEEE Robotics and Automation Letters*, vol. 5, no. 2, pp. 1656–1663, 2020.
- [11] M. Damani, Z. Luo, E. Wenzel, and G. Sartoretti, "Primal\_2: Pathfinding via reinforcement and imitation multi-agent learning-lifelong," *IEEE Robotics and Automation Letters*, vol. 6, no. 2, pp. 2666–2673, 2021.
- [12] X. Chen, Z. Xiao, Y. Cheng, C.-C. Hsia, H. Wang, J. Xu, S. Xu, F. Dang, X.-P. Zhang, Y. Liu, *et al.*, "Soscheduler: Toward proactive and adaptive wildfire suppression via multi-uav collaborative scheduling," *IEEE Internet of Things Journal*, vol. 11, no. 14, pp. 24 858–24 871, 2024.
- [13] B. Yamauchi, "Frontier-based exploration using multiple robots," in *Proceedings of the International Conference on Autonomous Agents*, 1998, pp. 47–53.
- [14] M. Puig, J. Puig-Navarro, H. Garcia de Marina, *et al.*, "Distributed m-postman exploration with coordinates-free voronoi partitioning," in *IEEE International Conference on Robotics and Automation*. IEEE, 2015, pp. 5550–5555.
- [15] R. Zlot, A. Stentz, M. B. Dias, and S. Thayer, "Multi-robot exploration controlled by a market economy," in *Proceedings IEEE International Conference on Robotics and Automation*, vol. 3. IEEE, 2002, pp. 3016–3023.
- [16] L. Liu and D. A. Shell, "Optimal market-based multi-robot task allocation via strategic pricing," in *Robotics: Science and Systems*, vol. 9, no. 1, 2013, pp. 33–40.
- [17] K. Masaba and A. Q. Li, "Gvgexp: Communication-constrained multi-robot exploration system based on generalized voronoi graphs," in *International Symposium on Multi-Robot and Multi-Agent Systems*. IEEE, 2021, pp. 146–154.
- [18] S. Koenig and M. Likhachev, "D\* lite," *Aaai/iaai*, pp. 476–483, 2002.
- [19] P. Bagad, P. Dahatonde, R. Gagare, I. Athare, and G. Ghule, "Optimizing pathfinding in dynamic environments: A comparative study of a\* and d-lite algorithms," in *IEEE Pune Section International Conference*, 2024, pp. 1–11.
- [20] C. Ferner, G. Wagner, and H. Choset, "Odrm\* optimal multirobot path planning in low dimensional search spaces," in *IEEE International Conference on Robotics and Automation*, 2013, pp. 3854–3859.
- [21] T. Fan, P. Long, J. Pan, *et al.*, "Distributed multi-robot collision avoidance via deep reinforcement learning for navigation in complex scenarios," in *The International Journal of Robotics Research*, vol. 39, no. 7, 2020, pp. 856–892.
- [22] Z. Ma, Y. Luo, and H. Ma, "Distributed heuristic multi-agent path finding with communication," in *IEEE International Conference on Robotics and Automation*, 2021, pp. 8699–8705.
- [23] Z. Chen, B. Subagdja, and A.-H. Tan, "End-to-end deep reinforcement learning for multi-agent collaborative exploration," in *IEEE International Conference on Agents*. IEEE, 2019, pp. 99–102.
- [24] J. Cao, Y. Wang, Y. Liu, and X. Ni, "Multi-robot learning dynamic obstacle avoidance in formation with information-directed exploration," *IEEE Transactions on Emerging Topics in Computational Intelligence*, vol. 6, no. 6, pp. 1357–1367, 2021.
- [25] X. Ye, Z. Deng, Y. Shi, and W. Shen, "Toward energy-efficient routing of multiple agvs with multi-agent reinforcement learning," *Sensors*, vol. 23, no. 12, p. 5615, 2023.
- [26] V. D. Sharma, J. Lee, M. Andrews, and I. Hadžić, "Hybrid classical/rl local planner for ground robot navigation," *arXiv preprint arXiv:2410.03066*, 2024.
- [27] W. Li, H. Chen, B. Jin, W. Tan, H. Zha, and X. Wang, "Multi-agent path finding with prioritized communication learning," in *International Conference on Robotics and Automation*, 2022, pp. 10 695–10 701.
- [28] G. Kahn, P. Abbeel, and S. Levine, "BADGR: An autonomous self-supervised learning-based navigation system," *IEEE Robotics and Automation Letters*, vol. 6, no. 2, pp. 1312–1319, 2021.
- [29] B. Wang, Z. Liu, Q. Li, and A. Prorok, "Mobile robot path planning in dynamic environments through globally guided reinforcement learning," *IEEE Robotics and Automation Letters*, vol. 5, no. 4, pp. 6932–6939, 2020.
- [30] A. Faust, K. Oslund, O. Ramirez, A. Francis, L. Tapia, M. Fiser, and J. Davidson, "Prm-rl: Long-range robotic navigation tasks by combining reinforcement learning and sampling-based planning," in *IEEE International Conference on Robotics and Automation*. IEEE, 2018, pp. 5113–5120.
- [31] A. Skrynnik, A. Andreychuk, K. Yakovlev, and A. I. Panov, "When to switch: planning and learning for partially observable multi-agent pathfinding," *IEEE Transactions on Neural Networks and Learning Systems*, 2023.
- [32] B. Yamauchi, "A frontier-based approach for autonomous exploration," in *Proceedings of the IEEE International Symposium on Computational Intelligence in Robotics and Automation*. IEEE, 1997, pp. 146–151.

- [33] H. W. Kuhn, "The hungarian method for the assignment problem," *Naval Research Logistics Quarterly*, vol. 2, no. 1-2, pp. 83–97, 1955.
- [34] A. Skrynnik, A. Andreychuk, K. Yakovlev, and A. Panov, "Decentralized monte carlo tree search for partially observable multi-agent pathfinding," in *Proceedings of the AAAI Conference on Artificial Intelligence*, vol. 38, no. 16, 2024, pp. 17 531–17 540.
- [35] E. Boyarski, A. Felner, R. Stern, G. Sharon, O. Betzalel, D. Tolpin, and E. Shimony, "Icbs: The improved conflict-based search algorithm for multi-agent pathfinding," in *Proceedings of the International Symposium on Combinatorial Search*, vol. 6, no. 1, 2015, pp. 223–225.